

Title	Investigation of the meandering bead formation process in metal inert gas welding
Author(s)	Aoyama, Kai; Komen, Hisaya; Tanaka, Manabu et al.
Citation	Welding in the World. 2025
Version Type	VoR
URL	https://hdl.handle.net/11094/103005
rights	This article is licensed under a Creative Commons Attribution 4.0 International License.
Note	

# The University of Osaka Institutional Knowledge Archive : OUKA

https://ir.library.osaka-u.ac.jp/

The University of Osaka

### **RESEARCH PAPER**



# Investigation of the meandering bead formation process in metal inert gas welding

Kai Aoyama<sup>1</sup> · Hisaya Komen<sup>1</sup> · Manabu Tanaka<sup>1</sup> · Kyohei Konishi<sup>2</sup> · Koichi Taniguchi<sup>2</sup> · Satoshi Igi<sup>2,3</sup>

Received: 25 March 2025 / Accepted: 14 August 2025 © The Author(s) 2025

### **Abstract**

In this study, the meandering bead formation process during a Metal Inert Gas Welding (MIGW) was investigated, and the factors causing bead meandering were identified. An experimental system with six tungsten cathodes arranged in a circular pattern, capable of linear movement in the radial direction, was used to simulate the behavior of the cathode spots and the molten wire during MIGW. As a result, it was observed that when there was a bias in the distribution of the cathode spots and the welding current, molten metal droplets detached from the wire tip were carried to the side opposite to where the cathode spots and welding current were concentrated. The correlation coefficients between the welding current bias and the angle of the molten metal column, as well as the droplet transport position, were 0.92 and 0.97, respectively, indicating a strong positive correlation. From these results, it was suggested that meandering bead formation during MIGW was caused by the molten metal droplets transported intensively away from the weld line due to unbalanced driving forces acting on the molten wire, which were caused by the unbalanced cathode spot distribution and welding current. It was suggested that in MIGW, the crawling behavior of the cathode spots induced the destabilization of the molten metal droplet transfer formed at the wire tip, leading to the formation of meandering beads.

Keywords Metal inert gas welding · Meandering bead · High-speed camera · Cathode spot · Metal transfer

### 1 Introduction

Gas Metal Arc Welding (GMAW) is a welding process in which a welding wire that is used as a consumable electrode is continuously supplied. The wire tip is heated and melted by Joule heating and heat transfer with the arc plasma, forming a molten metal droplet. The molten metal droplets are detached from the wire tip and transported to a weld pool as a heat input, and finally the joining is achieved when the molten metal solidifies after the heat source passed. This welding process is widely used in various industries because of its high deposition rate. GMAW is classified into Metal Active Gas Welding (MAGW) in which a mixture

gas contained active gases, such as  $O_2$  and  $CO_2$ , is used as the shielding gas, and Metal Inert Gas Welding (MIGW), in which inert gas such as Ar is used as the gas. During MAGW, O is mixed into the weld pool, and the toughness of the weld metal decreases [1–3]. On the other hand, MIGW is known to produce high-quality weld beads because the shield by inert gas prevents the oxidation and the nitridation of the weld metal. However, its application is limited to aluminum alloys that have a strong oxide film on the base metal surface, and it is difficult to apply it to carbon steels that have a relatively thin oxide film or no oxide film at all.

One of the factors limiting the range of applications of MIGW is the instability of the cathode spot when inert gas is used as shielding gas. Ushio et al. [4] reported that when an Ar- $O_2$  mixed gas containing a small amount of  $O_2$  was used as the shielding gas, an oxide layer was continuously formed on the weld pool surface and cathode spots occurred in a fixed area, resulting in stable welding. In contrast, they clarified that in MIGW, no oxide layer was formed on the weld pool surface, which led to the instability of the cathode spots and the formation of a meandering bead. In order to prevent the formation of the meandering beads, some

Published online: 27 August 2025



Hisaya Komen h.komen.jwri@osaka-u.ac.jp

Joining and Welding Research Institute, The University of Osaka, Osaka, Japan

<sup>&</sup>lt;sup>2</sup> JFE Steel Corporation, Chiba, Japan

Present Address: JFE Techno-Research Corporation, Kanagawa, Japan

welding technologies have been developed to suppress these unstable cathode point behaviors and unstable molten metal column behaviors. For example, Sakurai et al. [5] applied an external magnetic field to the arc plasma in a MIGW to control the cathode spot behavior and successfully suppressed the formation of meandering beads. Nakamura et al. [6–8] developed the coaxial hybrid solid wire to suppress the unstable molten metal column behavior and prevent the meandering bead formation. This wire had a core wire with a low melting point and a hoop material with a high melting point. The stable metal transfer was achieved by preferentially melted core wire, and the formation of the meandering bead was prevented.

In addition, in recent years, the use of high alloy components in line with the increase in material strength has made it difficult to ensure the required weld joint properties using conventional methods. For example, in automobile suspension parts using high-strength steel plates, the amount of slag (an oxide) generated increases, reducing the corrosion resistance of the weld joint, which is an issue [9]. To solve this problem, the MIGW stabilization technology for carbon steel has been developed. Konishi et al. [10] have used high current pulses to control the unstable molten metal droplet transfer in MIGW to periodic short-circuit transfer, making it possible to obtain high-quality weld beads without meandering.

In these previous studies, formation of the meandering bead was suppressed by preventing either unstable cathode spot behavior or unstable molten metal column behavior. However, the mechanisms of how these unstable behaviors of the cathode spot and the molten metal column affect meandering bead formation have not been clarified yet. In this study, the behaviors of the cathode spot and molten metal column were observed to clarify the effect of welding current bias on the molten metal column behavior. In addition, this study attempted to elucidate the mechanism of meandering bead formation based on the experimental results.

# 2 Experimental method

Figure 1 shows schematic illustrations of the experimental system developed in this study to simulate the cathode spot behavior during GMAW. Figure 1b shows an enlarged view of area A surrounded by the red dotted line in Fig. 1a. In the experimental system (Fig. 1b), a welding wire was used as the anode, six tungsten electrodes installed at 60 deg. intervals were used as cathodes, and arc plasma was generated between the electrodes [11]. Each tungsten cathode was placed on a jig equipped with a rack (Fig. 1c). A pinion attached to a stepping motor (Oriental motor, CRK-523PAKD) moved the rack linearly. The tungsten cathode

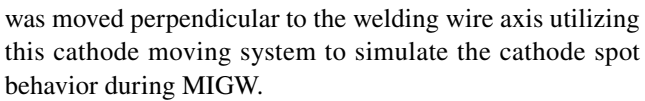


Table 1 shows experimental conditions for simulating cathode spot behavior during MIGW. 3.2 mm diameter W-2wt.%  $La_2O_3$  electrodes whose tip angle was set at 30 degrees were used as the cathode. As shown in Fig. 1b, the vertical distance between the contact and cathode tips was set to 25 mm. The distance between the tips of the tungsten electrodes facing each other was set to 6 mm.

Figure 2 shows a schematic illustration of the experimental setup used to observe the molten metal column while simulating the cathode spot behavior during MIGW. The molten metal column was captured using a color high-speed camera (Nac Image Technology, MEMRECAM ACS-1 M16). The camera consisted of a single-focus lens (Nikon, ED AF MICRO NIKKOR 200 mm 1:4 D), a teleconverter (Kenko, TELEPLUS HDpro 2X DGX), and two neutral density filters (Kenko, ND8). The frame rate, exposure time, and aperture value were set to 5,000 fps, 5.0 μs, and f/32, respectively. The currents flowing through the welding wire and each tungsten electrode during the experiment were measured using clamp meters (HIOKI, Clamp-On AC/DC HiTester model 3285 or CT7742 connected to CM7290) and data logger (KEYENCE NR-HV04).

This experimental system was utilized to quantitatively evaluate the behavior of a molten metal column when the welding current was concentrated on one side. Figure 3 shows the measurement parameters of the molten metal column used in this study. Argon and metal plasmas are shown in the red and blue regions, respectively. The dotted dashed lines indicate the central axes of the welding wire, molten metal column, droplets, and tungsten electrodes. The angle of the molten metal column,  $\theta$ , and the transport position of droplets, x, were measured from still images taken by a color high-speed camera using the image-processing software ImageJ [12, 13].

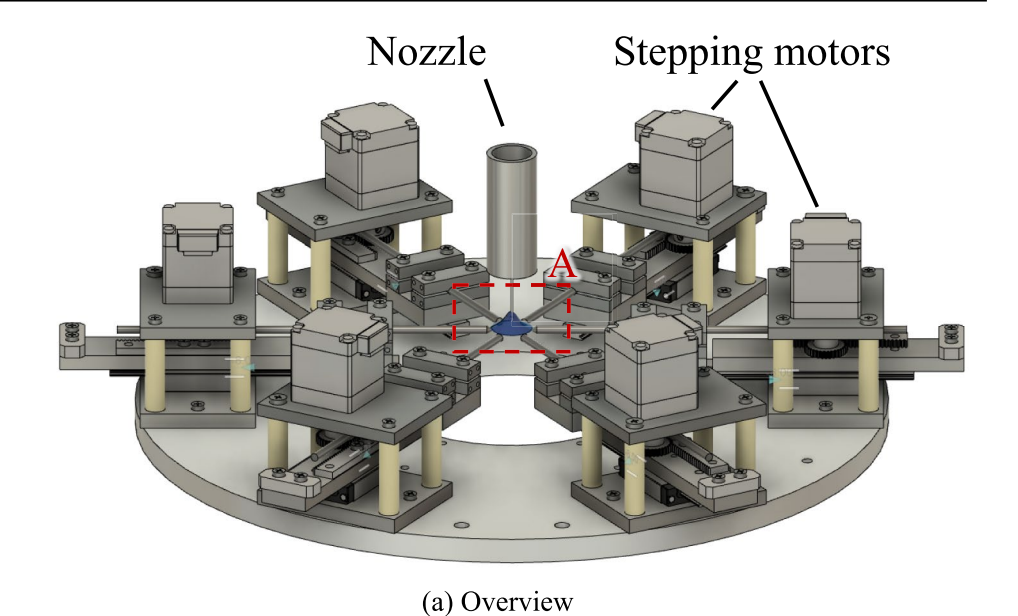
## 3 Results and discussion

# 3.1 Effect of cathode spot behavior on molten metal column behavior

To simulate cathode spot behavior using the developed experimental system, the cathode spot behavior during bead on plate welding was observed. The welding conditions shown in Table 1 were used and welding speed was set to 10 mm/s. The base metal was mild steel with the mill scale removed. Figure 4 shows the behavior of the cathode spot when Ar + 2%  $O_2$  mixture gas is used as the shielding gas. In this figure, each time shows relative time from Fig. 4a, and the red circles indicate the areas of cathode spot movement



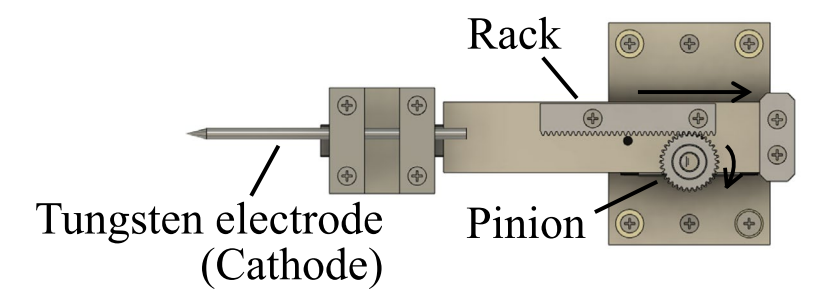
**Fig. 1** Experimental setup for simulating cathode spot behavior in MIGW



Welding wire (Anode)
Arc plasma
6 mm

# Tungsten electrodes (Cathode)

(b) Magnified view of area A in Fig. 1(a)



(c) Mechanism for direct movement of the tungsten electrode

on the base metal surface. As shown in Fig. 4, the areas of cathode spot movement were symmetrically distributed around the molten metal column when Ar + 2%  $O_2$  mixture gas was used as the shielding gas. This was thought to be due

to the formation of an oxide layer on the base metal surface by  $O_2$  in the shielding gas, and cathode spot was preferentially generated on the oxide layer. Figure 5 shows the bead

Moving direction



Table 1 Experimental conditions for simulating cathode spot behavior

Setting welding current	250 A
Setting arc voltage	27 V
Polarity	DCEP (direct current elec- trode positive)
Wire	MIX-50S (JIS Z 3312 YGW16), φ 1.2 mm
Shielding gas	100% Ar
Gas flow rate	25 L/min
Nozzle inner diameter	16.0 mm
Cathode material	W-2wt.%La <sub>2</sub> O <sub>3</sub>
Cathode diameter	3.2 mm
Cathode tip angle	30 deg
Vertical distance of contact tip from cathode tips	25 mm
Distance between facing electrodes	6 mm

appearance in this condition. As reported in the previous study [4], the weld bead without meandering was formed.

Figure 6 shows observation results of cathode spot behavior when 100% Ar gas was used as the shielding gas. The same as Fig. 4, each time shows relative time from Fig. 4a and the red circles indicate the areas of cathode spot movement on the base metal surface. As shown in Fig. 6, the cathode spot that was generated on the base metal surface (at a distance from the center axis of the molten metal column) moved over time when 100% Ar gas was used as the shielding gas because there was no oxide layer on the base metal

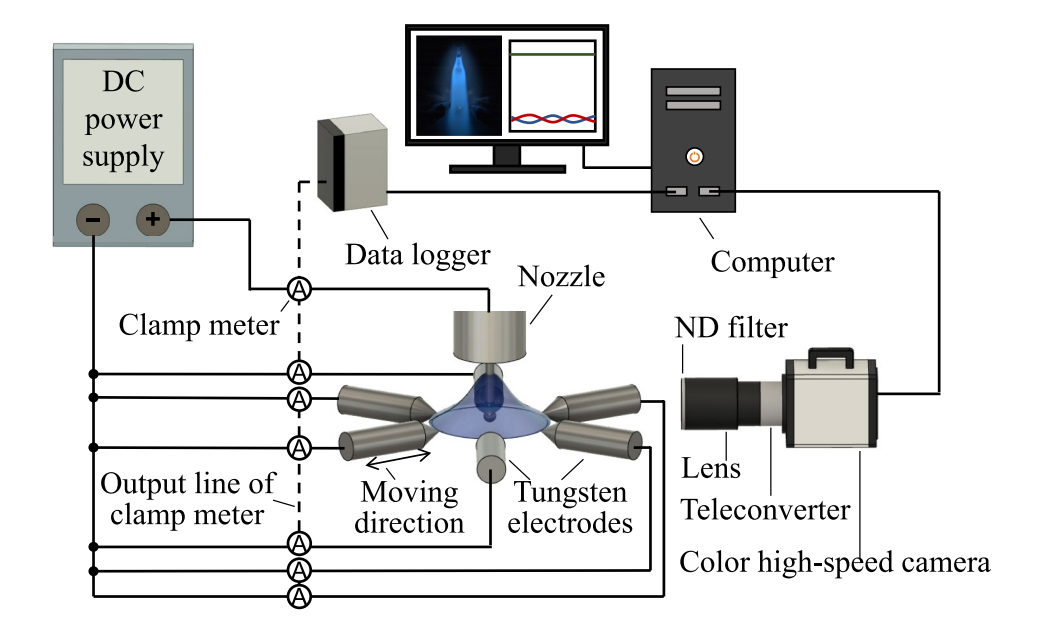
surface. Therefore, the cathode spots were widely distributed when 100% Ar was used as the shielding gas. Figure 7 shows the bead appearance in this condition. In this condition, the meandering bead was formed.

Figure 8 shows the behavior of tungsten electrodes used to simulate the cathode spot behavior during GMAW. As shown in Fig. 8a, each tungsten electrode was assigned a number from one to six. As shown in Fig. 4, the area of the cathode spot movement was symmetrically fixed to the molten metal column when Ar + 2%  $O_2$  mixture gas was used as the shielding gas. Therefore, tungsten electrodes fixed at their initial positions were utilized to simulate the cathode spot behavior with the Ar + 2%  $O_2$  mixture gas as the shielding gas, as shown in Fig. 8a.

On the other hand, the cathode spot behavior when 100% Ar gas was used as shielding gas was simulated by the movement of the tungsten electrodes. Furthermore, the red arrows show the direction in which tungsten electrodes are moved, and the red squares show the state in which tungsten electrodes are stopped. Figure 8a shows the moment at which tungsten electrode no. 1 started to move. Each tungsten electrode (nos. 1–6) was moved away from the facing tungsten electrode every 30 ms. Additionally, each tungsten electrode was returned to its initial position after moving by 4 mm. As shown in Fig. 8c, tungsten electrode no. 4 was controlled to move away from the facing tungsten electrode no. 1 when tungsten electrode no. 1 returned to its initial position. The tungsten electrodes facing each other were moved together (in pairs) to simulate the cathode spot behavior with 100% Ar used as the shielding gas.

Figure 9 shows the behavior of the molten metal column when the cathode spot behavior of  $Ar + 2\% O_2$  mixture gas as the shielding gas was simulated using tungsten electrodes. In this experiment, the welding current was defined as I, and the currents flowing to tungsten electrode nos. 2 and

Fig. 2 Schematic illustration of setup for observation of molten wire in the experiment of simulating cathode spot behavior





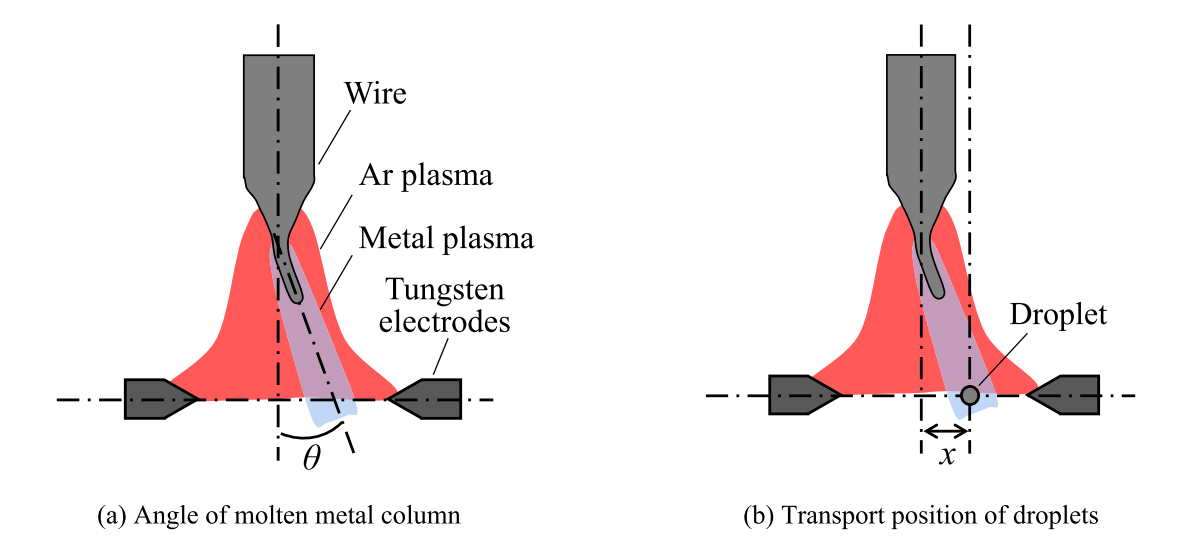
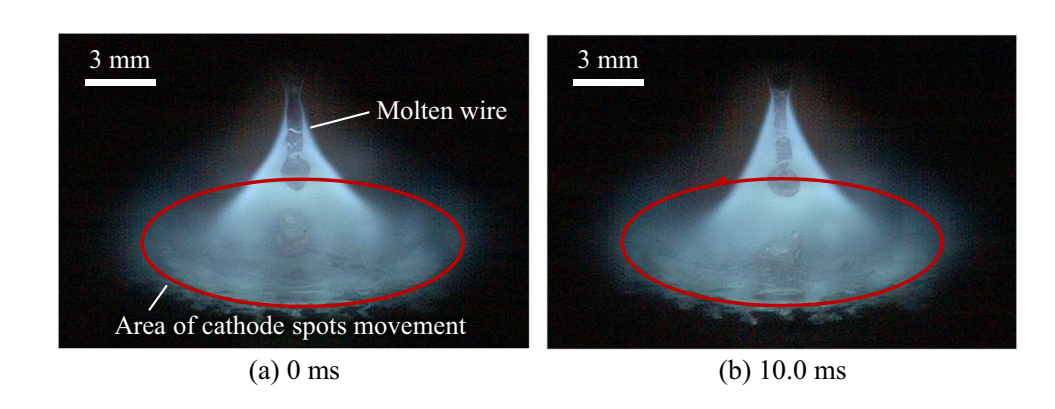


Fig. 3 Schematic illustration of measurement items in the observation of molten metal column

**Fig. 4** Cathode spot behavior of bead on plate welding using Ar+2% O<sub>2</sub> as shielding gas



# Welding direction

Fig. 5 Weld bead appearance obtained by bead on plate welding using  $Ar + 2\% O_2$  as shielding gas

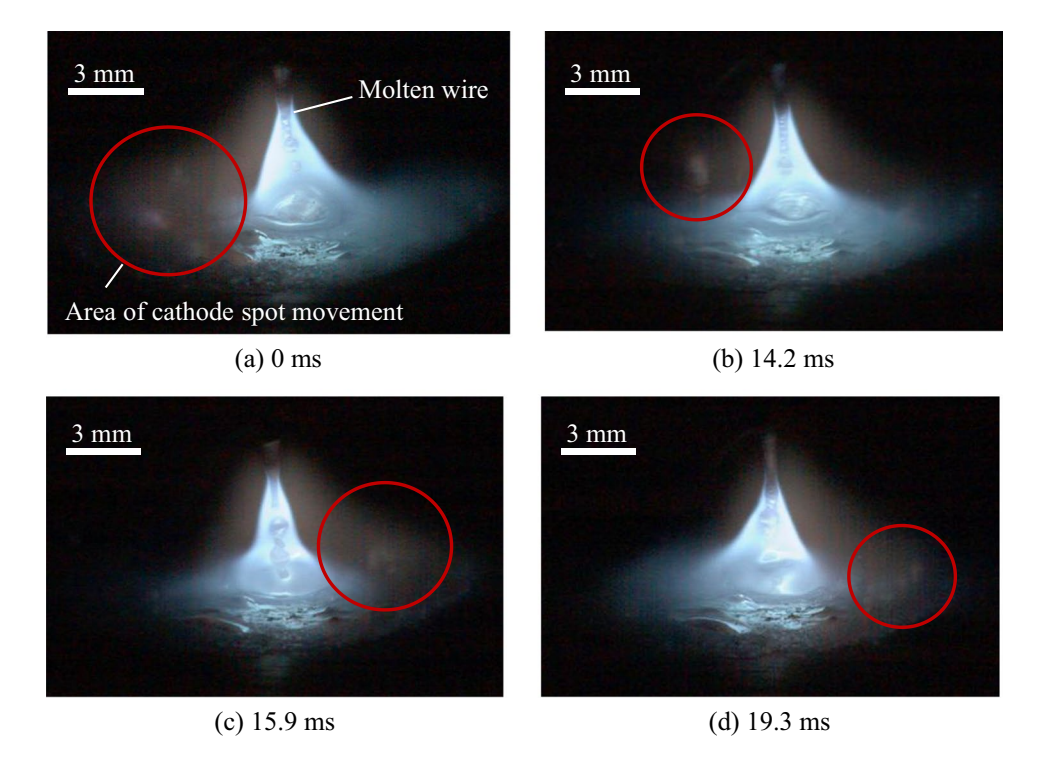
5 were defined as  $I_1$  and  $I_2$ , respectively. As shown in this figure, stable molten metal column behavior without bending in the radial direction of the wire was observed, when the cathode spot behavior in MAGW using Ar + 2%  $O_2$  mixture gas as the shielding gas was simulated with the tungsten electrodes. Figure 10 shows the measurement results for the welding current I and currents  $I_1$  and  $I_2$  flowing to tungsten electrode nos. 2 and 5, respectively, which were set perpendicular to the shooting direction. This figure confirms that

the currents flowing through each tungsten electrode were almost constant.

Figure 11 shows the molten metal column behavior when the cathode spot behavior during welding using 100% Ar as the shielding gas was simulated using tungsten electrodes. Figure 12 shows the measurement results of the currents flowing in the welding wire and tungsten electrode nos. 2 and 5. At 0 s, shown on the horizontal axis, the tungsten electrodes began to move. The black dashed lines indicate the time from  $t_0$  to  $t_3$  shown in Fig. 11. As shown in Fig. 12, the currents flowing through the tungsten electrodes were changed with the movement of the electrodes. As shown in Figs. 11 and 12, the tungsten electrode no. 2 was moved toward the welding wire over time, and the current flowing through the electrode increased. On the other hand, it was confirmed that the tungsten electrode no. 5 was moved away from the welding wire over time, and the current flowing through the electrode decreased. The molten metal column flowed to the opposite side of tungsten electrode no. 5, where the current increased at  $t_1$ . Similar molten metal column behavior was observed at  $t_3$ . These results suggested



**Fig. 6** Cathode spot behavior of bead on plate welding using 100% Ar as shielding gas



# Welding direction



**Fig. 7** Weld bead appearance obtained by bead on plate welding using 100% Ar as shielding gas

that the molten metal column during bead on plate welding was affected by unstable cathode spot behavior.

# 3.2 Effect of welding current bias on molten metal column behavior

The relationship between the welding current bias and molten metal column behavior was investigated to quantitatively evaluate the effect of the cathode spot behavior on the molten metal column behavior. Figure 13 shows the movement of the tungsten electrodes used to investigate the effect of the welding current bias on the molten metal column behavior. As shown in this figure, tungsten electrode nos. 1–3 were fixed, and tungsten electrode nos. 4–6 were moved away from the welding wire. Through these movements, the welding current was concentrated on electrode nos. 1–3. Then, the evolution in the transport position of

droplets, x, and the angle of molten metal column,  $\theta$ , with time were measured.

Figure 14 shows the results for the molten metal column when the welding current was concentrated on one side. Figure 15 shows the measured results of the currents flowing in the welding wire and tungsten electrode nos. 2–5 in this experiment. Figure 16 shows the percentage of the total current flowing through tungsten electrodes 1–3. As same as Fig. 12, the 0 s shown in Figs. 15 and 14 are the moments when the tungsten electrodes were started to move. Each dashed line indicates the time at which the observation results shown in Fig. 14 were obtained.

As shown in Fig. 14, when tungsten electrode nos. 4–6 moved away from the welding wire, the molten metal column flowed in the direction of motion of tungsten electrodes. As shown in Fig. 15, the current  $I_2$  flowing to tungsten electrode no. 5 decreased as tungsten electrode nos. 4–6 moved away from the welding wire. Furthermore, it was confirmed from Fig. 16 that the percentage of current flowing to the tungsten electrode nos. 1–3 increased from approximately 50% to approximately 100% as the tungsten electrode nos. 4–6 moved away from the wire.

Figure 17 shows the measurement result of the angle of molten metal column  $\theta$  when the welding current was concentrated on one side. The horizontal axis in this figure shows the percentage of the total current flowing through the tungsten electrodes nos. 1–3, and the vertical axis shows the angle of molten metal column  $\theta$ . This



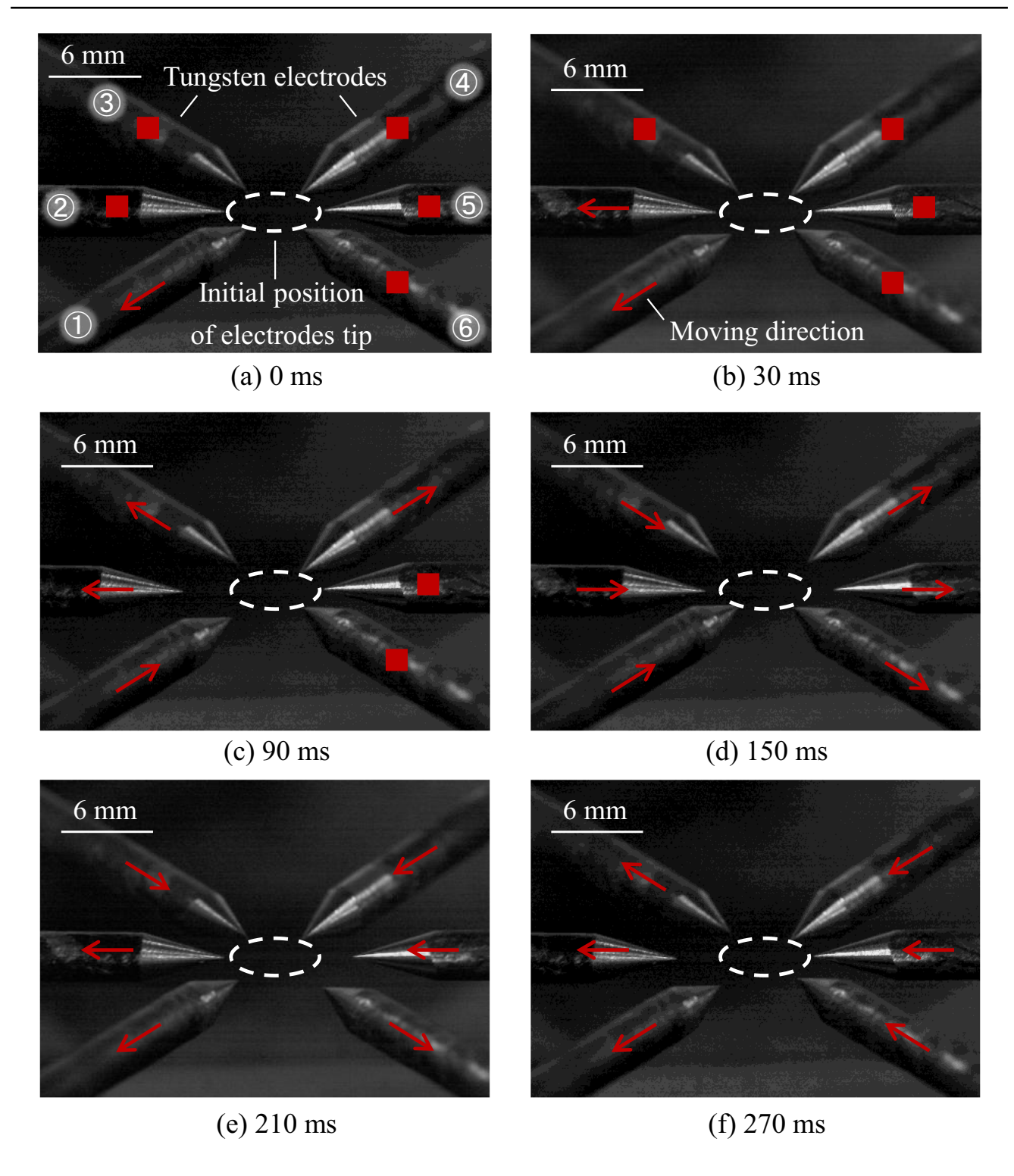


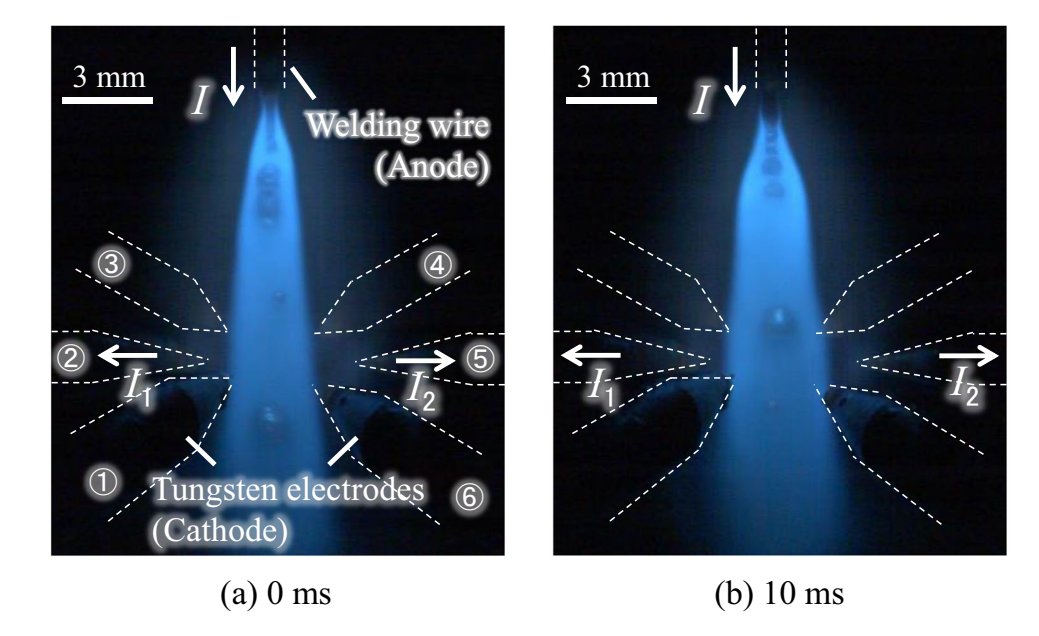
Fig. 8 Movement of tungsten electrodes for simulating cathode spot behavior during bead on plate welding

figure confirms that the angle of the molten metal column increased as the percentage of current flowing through the tungsten electrode nos. 1–3 increased. Using this result, the correlation coefficient between the welding current

bias and  $\theta$  obtained from Eq. (1) [14] was 0.92, confirming a strong positive correlation.



Fig. 9 Molten metal column in the experiment of simulating cathode spot behavior when Ar+2% O<sub>2</sub> mixture gas was used as shielding gas



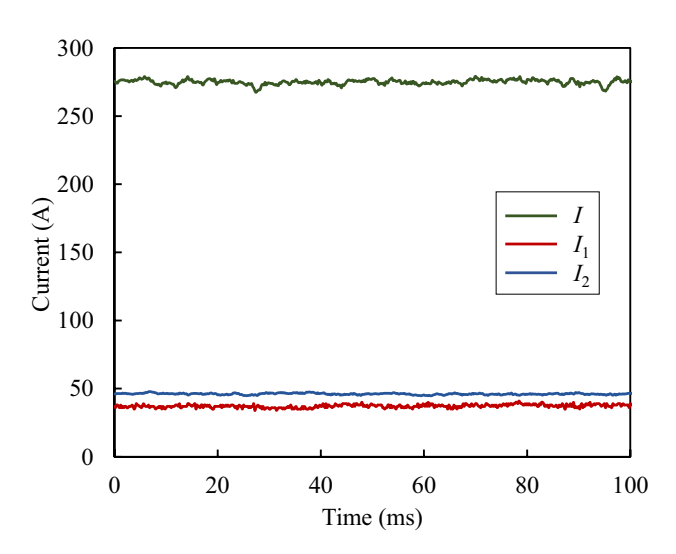


Fig. 10 Current waveforms in the experiment of simulating cathode spot behavior when Ar + 2%  $O_2$  mixture gas was used as shielding gas

$$r = \frac{\sum_{i} (x_i - \overline{x})(y_i - \overline{y})}{\sqrt{\sum_{i} (x_i - \overline{x})^2 \cdot \sum_{i} (y_i - \overline{y})^2}},$$
(1)

where r is the correlation coefficient (-), x is the welding current bias (%), and y is measured values, the angle of molten metal column (deg.) and transport position of droplets (mm).

Figure 18 shows the measurement results of the transport position of the droplets x when the welding current was concentrated on one side. The horizontal axis of this figure shows the percentage of the total current flowing through tungsten electrode nos. 1–3, and the vertical axis shows the transport position of the droplets x. From this figure, it was confirmed

that the molten metal droplets were transported away from the central axis of the welding wire as the percentage of current flowing through the tungsten electrode nos. 1–3 increased. The correlation coefficient between the welding current bias and the transport position of the droplets was 0.97, and a strong positive correlation was confirmed.

These results confirm that the molten metal droplets were transported away from the central axis of the welding wire when the welding current was concentrated on one side. These experimental results were discussed with a focus on the forces acting on the molten metal column. Figure 19 shows the schematic illustrations of process of unbalanced forces that acted on the molten metal column when the welding current was concentrated on one side. As shown in Fig. 19a, an arc plasma with the spray transfer mode during MIGW was separated into argon and metal plasmas, and the welding current preferentially flowed to the argon plasma, which had a high temperature and electrical conductivity [15]. When the welding current I(A) was concentrated on one side, the magnetic flux density vector  $\vec{B}$  (T) given by the Ampère's law (Eq. (2)) was generated asymmetrically along the central axis of the welding wire (Fig. 19b). As shown in Fig. 19c, the Lorentz force vector  $\vec{F}$  (N), expressed in Eq. (3), also acted asymmetrically on the molten metal column along the axis.

$$\vec{B} = \frac{\mu I}{2\pi r},\tag{2}$$

$$\vec{F} = \vec{j} \times \vec{B},\tag{3}$$

where  $\mu$  is the permeability (H/m), r is the distance from the current (m), and  $\vec{j}$  is the current density vector (A/m<sup>2</sup>). Furthermore, from the Bernoulli equation shown in Eq. (4), the



Fig. 11 Molten metal column in the experiment of simulating cathode spot behavior using 100% Ar as shielding gas

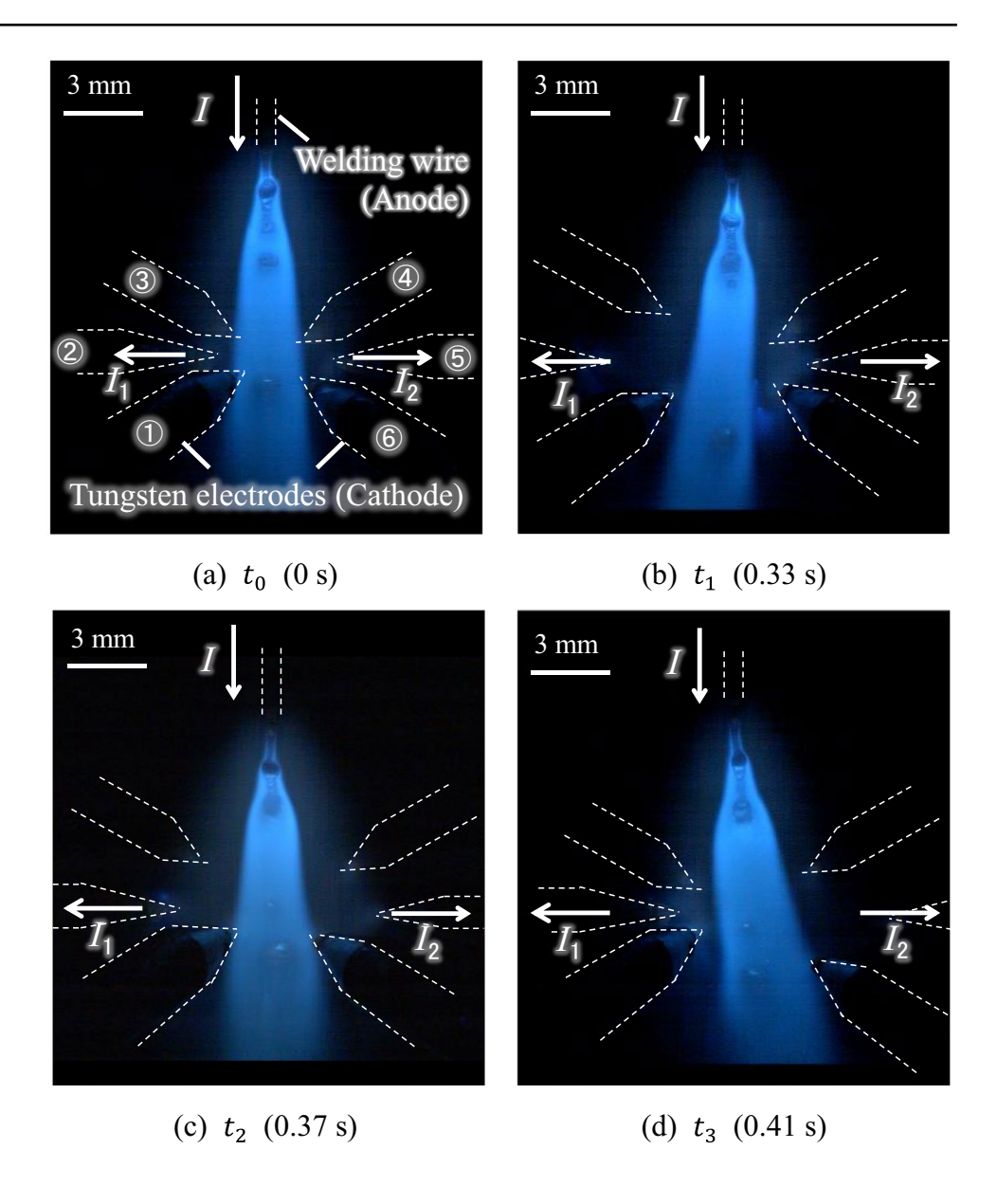
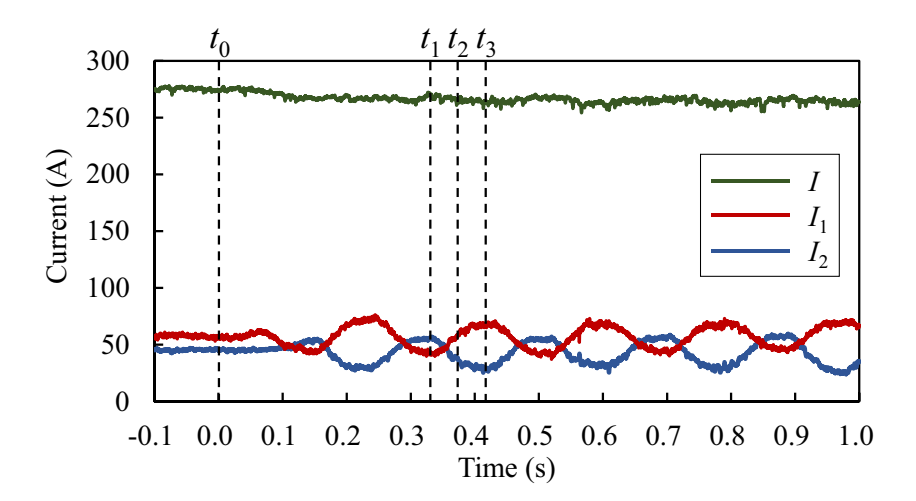
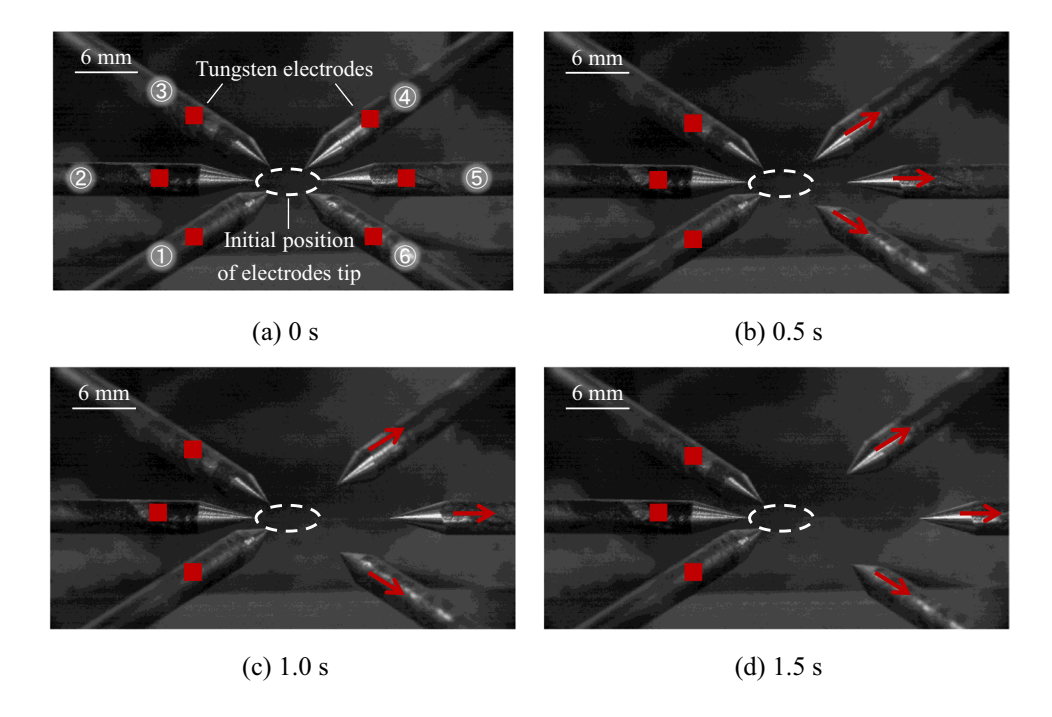


Fig. 12 Current waveforms in the experiment of simulating cathode spot behavior when 100% Ar gas was used as shielding gas





**Fig. 13** Movement of tungsten electrodes for the concentration of welding current on one side



arc pressure P (Pa) increased at the point where the plasma flow changed its direction when the velocity vector  $\vec{v}$  (m/s) of the plasma flow, the fluid density  $\rho$  (kg/m<sup>3</sup>), and the height z (m) on the same streamline were assumed constants.

$$P + \frac{1}{2}\rho |\vec{v}|^2 + \rho gz = \text{const.}$$
 (4)

Here, *g* is gravitational acceleration (m/s²). Therefore, when the streamline of a high-speed plasma flow is affected by a strong Lorentz force, the arc pressure is higher when the direction of the flow changes. Using these asymmetric Lorentz forces and arc pressures, the molten metal column flowed in the direction opposite to the welding current concentration, and the molten metal droplets were transported away from the central axis of the welding wire (Fig. 19e). When welding current bias is absent, the Lorentz force and arc pressure were considered to act almost symmetrically. The molten metal column, subjected to axisymmetric forces, grew almost along the wire center axis, and the molten metal droplets were thought to be transported near the central axis (Fig. 19f).

As stated above, it was suggested that meandering bead formation during MIGW was caused by the molten metal droplets transported intensively away from the weld line due to unbalanced driving forces acting on the molten wire, which were caused by the unbalanced cathode spot distribution and welding current.

### 4 Conclusions

In this study, the behaviors of the cathode spot and molten metal column were observed to clarify the effect of welding current bias on the molten metal column behavior. In addition, this study attempted to elucidate the mechanism of meandering bead formation based on the experimental results. The results of this study are summarized as follows:

Behavior of the molten metal column when the cathode spot behavior of Ar + 2% O<sub>2</sub> mixture gas as the shielding gas was simulated using tungsten electrodes. As a result, stable molten metal column behavior was observed, and the currents flowing through each tungsten electrode were almost constant. On the other hand, when the cathode spot behavior during welding using 100% Ar as the shielding gas was simulated using tungsten electrodes, it was confirmed that the molten metal column was curved as the tungsten electrodes moved, and the current flowing through each tungsten electrode was changed.



**Fig. 14** Molten metal column behavior when welding current was concentrated on one side

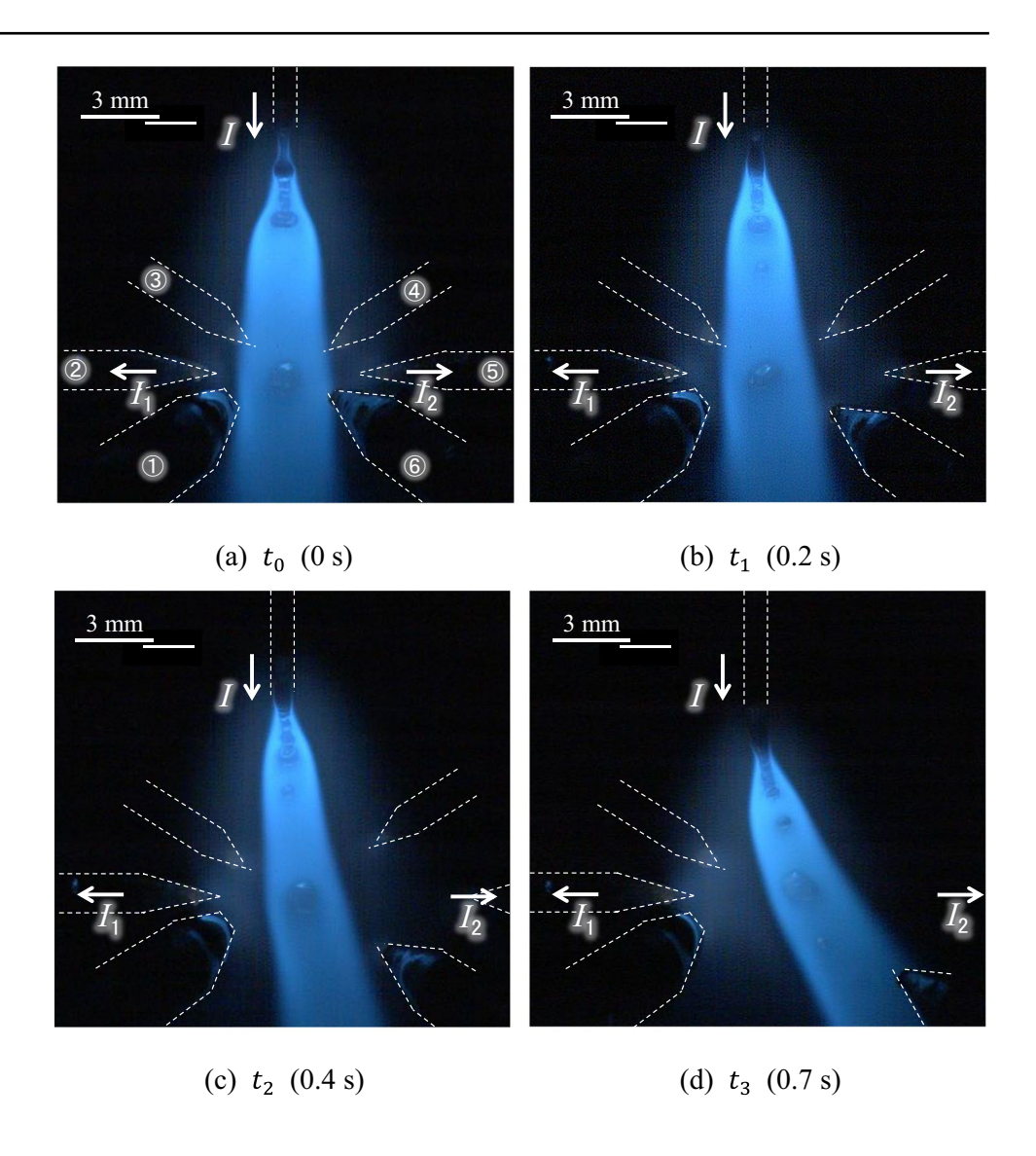


**Fig. 15** Current waveforms when welding current was concentrated on one side

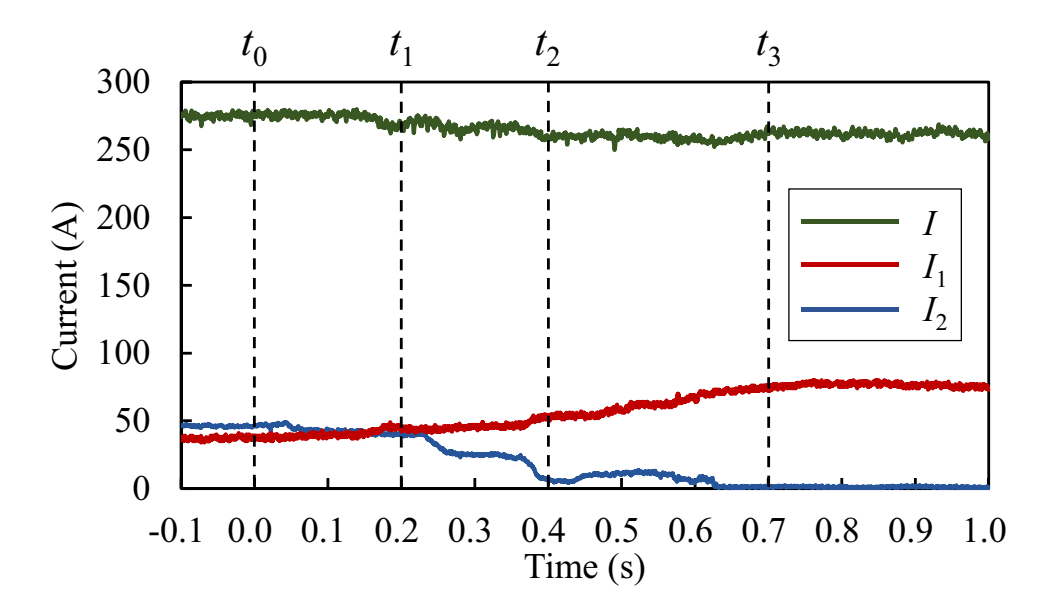
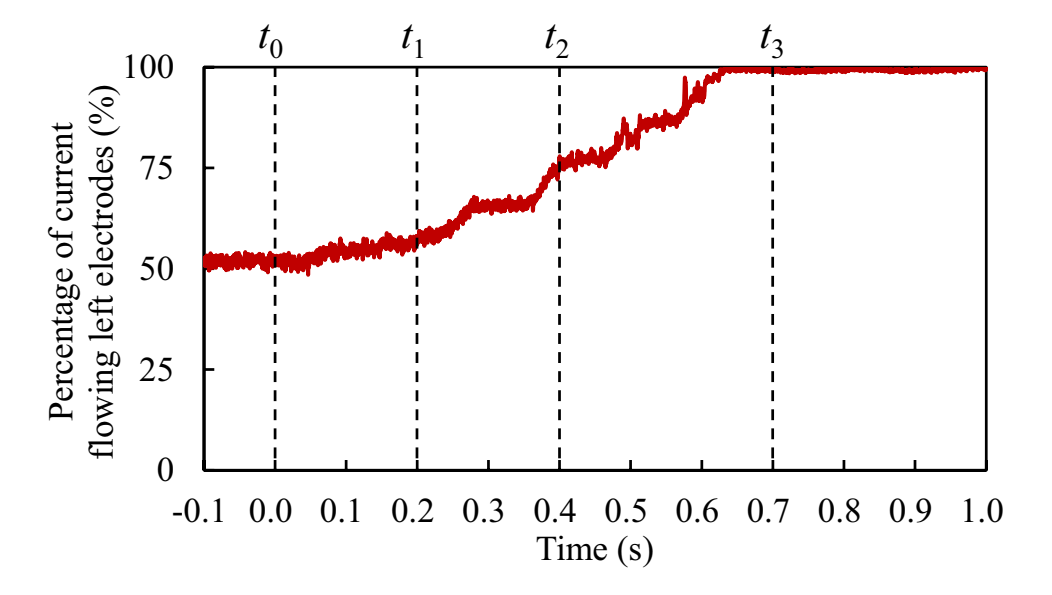




Fig. 16 Percentage of current flowing left electrodes when welding current was concentrated on one side



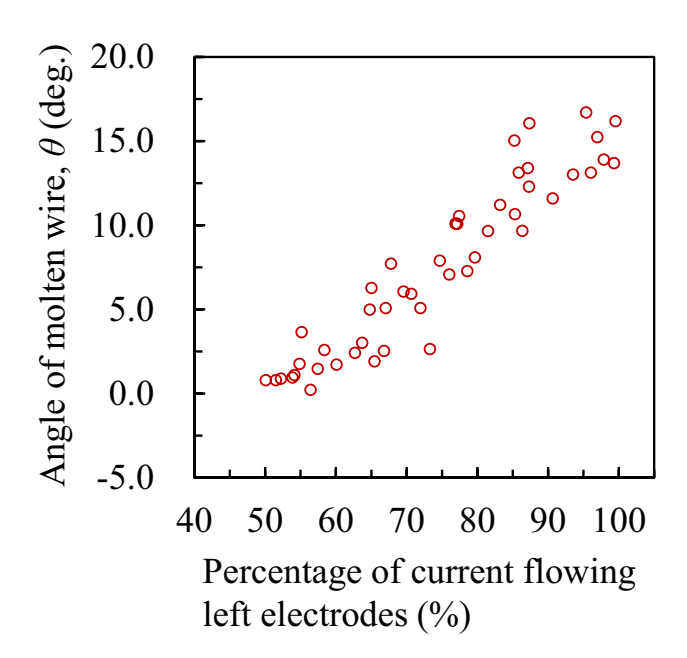
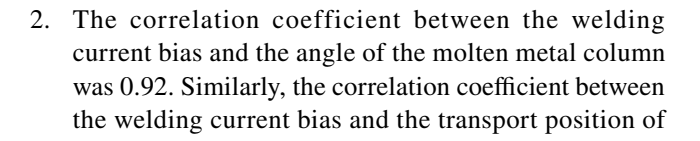


Fig. 17 Angle of molten metal column for different percentages of current flowing left electrodes



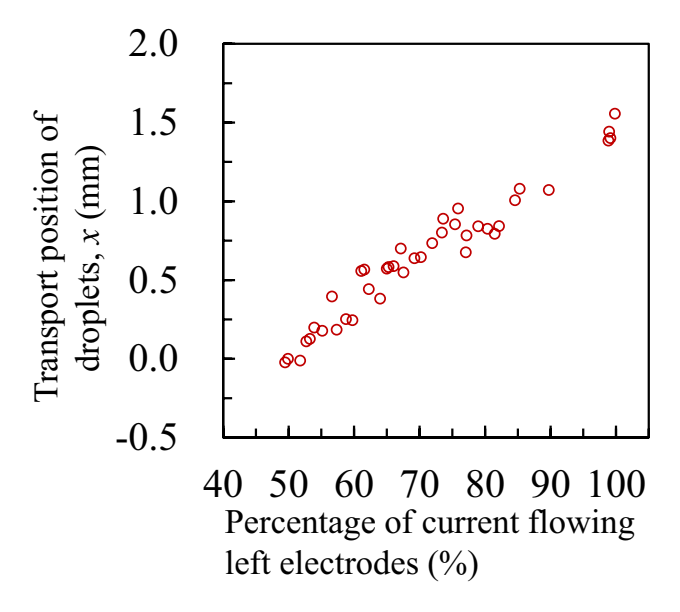
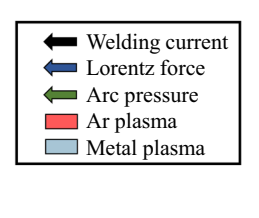
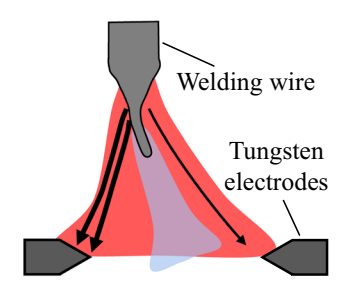


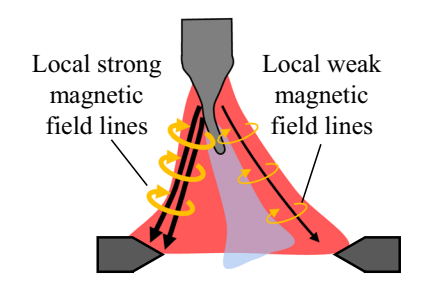
Fig. 18 Transport position of droplets for different percentages of current flowing left electrodes

- the droplets was 0.97, and strong positive correlations were confirmed.
- 3. When the welding current was concentrated on one side, the molten metal column flowed in the direction opposite to the welding current concentration using asymmetric Lorentz forces and arc pressures, and the molten metal droplets were transported away from the central axis of the welding wire.

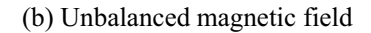


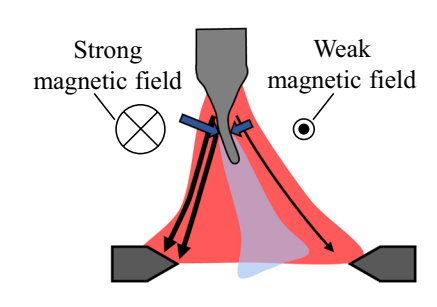


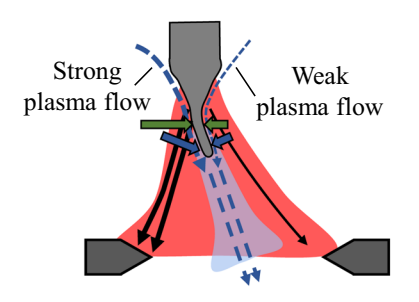




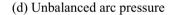
(a) Concentration of welding current

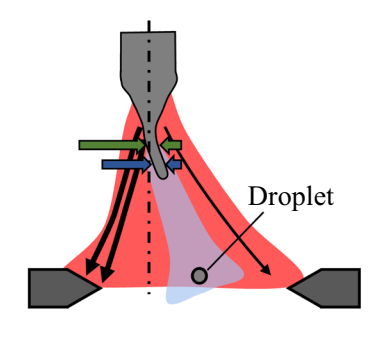


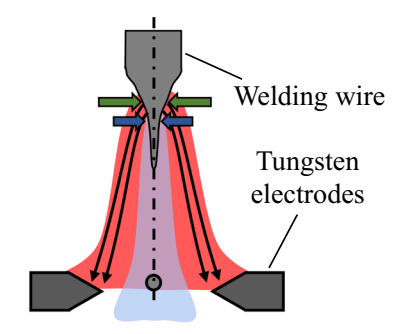




(c) Unbalanced Lorentz force







(e) Molten metal behavior when welding current was concentrated on one side

(f) Molten metal behavior when welding current flowed on both sides

Fig. 19 Influence of welding current concentration on molten metal column behavior



Author contribution Conceptualization: Kai Aoyama, Hisaya Komen, and Manabu Tanaka; methodology: Kai Aoyama and Hisaya Komen; material preparation and data collection: Kai Aoyama; validation: Kai Aoyama, Hisaya Komen, Manabu Tanaka, Kyohei Konishi, Koichi Taniguchi, and Satoshi Igi; writing—original draft preparation: Kai Aoyama; writing—review and editing: Kai Aoyama, Hisaya Komen, Manabu Tanaka, Kyohei Konishi, Koichi Taniguchi, and Satoshi Igi; supervision: Manabu Tanaka. All the authors have read and agreed to the published version of the manuscript.

Funding Open Access funding provided by The University of Osaka.

**Data availability** The data that support the findings of this study are available from the corresponding author upon reasonable request.

### **Declarations**

Competing interests The authors declare no competing interests.

Open Access This article is licensed under a Creative Commons Attribution 4.0 International License, which permits use, sharing, adaptation, distribution and reproduction in any medium or format, as long as you give appropriate credit to the original author(s) and the source, provide a link to the Creative Commons licence, and indicate if changes were made. The images or other third party material in this article are included in the article's Creative Commons licence, unless indicated otherwise in a credit line to the material. If material is not included in the article's Creative Commons licence and your intended use is not permitted by statutory regulation or exceeds the permitted use, you will need to obtain permission directly from the copyright holder. To view a copy of this licence, visit http://creativecommons.org/licenses/by/4.0/.

# References

- Witherell CE, Peck JV (1964) Progress in welding 9% nickel steel. Weld J 43(11):473s–480s
- Terashima S, Bhadeshia HKDH (2006) Changes in toughness at low oxygen concentrations in steel weld metals. Sci Technol Weld Joining 11(5):509–516. https://doi.org/10.1179/174329306X113299
- 3. Ito Y, Nakanishi M, Komizo Y (1982) Effects of oxygen on low carbon steel weld metal. Met Constr 14(9):472–478
- 4. Ushio M, Matsuda F (1978) Effect of oxygen on stabilization of arc in 9%Ni-steel GMA welding. Trans JWRI 7(1):93–100
- Sakurai N, Kaneko Y (2020) Study on suppression of bead-meandering of pure Ar-MIG arc welding using external magnetic field. Q J Jpn Weld Soc 38(2):69s-73s. https://doi.org/10.2207/qjjws.38.69s

- Nakamura T, Hiraoka K, Tanaka M (2010) Control of wire melting behavior using coaxial hybrid solid wire. Q J Jpn Weld Soc 29(3):35s-38s. https://doi.org/10.2207/qijws.29.35s
- Nakamura T, Hiraoka K (2009) Modelling of wire melting behaviour of coaxial hybrid solid wire in gas metal arc welding in a pure argon shielding gas. Weld World 53(7–8):R158–R165. https://doi.org/10.1007/BF03266727
- Nakamura T, Hiraoka K, Zenitani S (2008) Improvement of MIG welding stability in pure Ar shielding gas using small amount of oxygen and coaxial hybrid solid wire. Sci Technol Weld Joining 13(1):25–32. https://doi.org/10.1179/174329307X249289
- Yamamoto S, Suzuki S, Ando S, Ikeda R, Kataoka T (2018) Corrosion behavior of arc welded joints of chassis parts and an approach to improve its corrosion resistance. Q J Jpn Weld Soc 36(1):77s–85s. https://doi.org/10.2207/qjjws.36.77(inJapanese)
- Konishi K, Matsuda H, Sawanishi C, Igi S (2022) Stabilization of short-circuit transfer in pulse MIG welding for carbon steel -Development of slag-less pulse MIG welding technology for hotrolled ultra-high strength steel-. Prepr. National Meet. JWS 111. https://doi.org/10.14920/jwstaikai.2022f.0\_32 (in Japanese)
- Sato Y, Ogino Y, Sano T (2024) Process parameters and their effect on metal transfer in gas metal arc welding: a driving force perspective. Weld World 68(4):905–913. https://doi.org/10.1007/ s40194-023-01670-9
- Abramoff MD, Magelhaes PJ, Ram SJ (2004) Image processing with ImageJ. Biophotonics Int 11(7):36–42
- Schneider CA, Rasband WS, Eliceiri KW (2012) NIH Image to ImageJ: 25 years of image analysis. Nat Methods 9(7):671–675. https://doi.org/10.1038/nmeth.2089
- Ahlgren P, Jarneving B, Rousseau R (2003) Requirements for a cocitation similarity measure, with special reference to Pearson's correlation coefficient. J Am Soc Inf Sci Technol 54(6):550–560. https://doi.org/10.1002/asi.10242
- Shigeta M, Nakanishi S, Tanaka M, Murphy AB (2017) Analysis of dynamic plasma behaviours in gas metal arc welding by imaging spectroscopy. Weld Int 31(9):669–680. https://doi.org/10.1080/09507116.2016.1223220

**Publisher's Note** Springer Nature remains neutral with regard to jurisdictional claims in published maps and institutional affiliations.

